

Absorption properties of lipid-based substances by non-invasive fast mid-infrared imaging

Tim Kümmel^{1,4}, Tobias Teumer^{1,3}, Patrick Dörnhöfer¹,
Steffen Manser^{1,4}, Sascha Heinrich¹, Andreas Hien^{1,4}, Jürgen Marx²,
Frank-Jürgen Methner³, Matthias Rädle¹, and Björn Wängler⁴

¹ Mannheim University of Applied Sciences,
Center for Mass Spectrometry and Optical Spectroscopy,
Paul-Wittsack-Str. 10, 68163 Mannheim, Germany

² Scanovis GmbH,
An der Königsbach 8, 56075 Koblenz, Germany

³ Technische Universität Berlin,
Institute of Food Technology and Food Chemistry,
Seestraße 13, 13353 Berlin, Germany

⁴ University of Heidelberg,
Medical Faculty Mannheim,
Theodor-Kutzer-Ufer 1-3, 68167 Mannheim, Germany

Abstract In this study, we present a new optical non-contact measurement method, which is based on general characteristics of a flying-spot scanner. The focus is on the mapping of lipid-based substances, especially the scanning of fingerprints. The assessing of human fingerprints is conducted by using two lasers emitting in different selected wavelengths. Images generated by using these wavelengths comprise absorption information of the examined sample. By using image-processing and conversion algorithms, the lipid-based substances in the detected image section could not only be captured, but also displayed three-dimensionally. The setup of the optical scanning method presented here utilizes the mid infrared region, especially the wavelength range between 3 μm up to 4 μm . It was optimized in order to scan an area up to 50 cm^2 , with a spatial resolution of 20 μm and a data rate of 300 kS/s. Our data shows that mapping of human fingerprints can be performed by using the described

DOI: 10.58895/ksp/1000087509-3 erschienen in:

**OCM 2019 - 4th International Conference on Optical Characterization of Materials,
March 13th – 14th, 2019, Karlsruhe, Germany**

DOI: 10.58895/ksp/1000087509 | <https://www.ksp.kit.edu/site/books/m/10.58895/ksp/1000087509/>

method. Furthermore, a processing of the data set results in topographical information.

Keywords: Mid-infrared, scanning, absorption, lipids, non-invasive, human fingerprint, papillary ridge.

1 Introduction

Dactyloscopy is a person identification method recognised by science and jurisprudence. It deals with the recording and evaluation of human fingerprints [1]. Dactyloscopic marks are unique, unchangeable and classifiable. Due to these properties, they are particularly suitable for use in forensic technology. Dactyloscopic marks at crime scenes are created in the form of imprints, both latently by the excretion of skin's own substances, e.g. finger fat, and by the transfer of exogenous substances. Fingerprints are created by the papillary ridges on the fingertip. Each finger has a unique pattern. These patterns remain the same for a lifetime. Fingerprints can be classified into different pattern types. For this purpose, part of the total imprint is determined as the pattern area [2]. Forensically, general papillary line progressions and conspicuous structures are investigated [2,3]. These structures form the basis for the dactyloscopic proof of identity. The shape and position of the features in relation to each other represent primary importance [3]. Conspicuous structures on fingertips such as scars, wrinkles and furrows are also examined.

In practice, optical [4,5], physical [4] and chemical methods [6,7] are used to make a fingerprint visible. In certain specific cases, it is possible to search and to visualize finger marks in one step, however the original mark is destroyed in this approach [4–8]. In other cases, the finger mark securing can be performed at the same time [6]. The (substrate) material, its surface condition and its substance are important components in the selection of a suitable process [5].

The detection of finger marks by means of optical methods is contactless and non-destructive [4,5]. However, this method demands long measurement periods [9]. Therefore, we present a non-contact scanning measurement method providing fingerprints for rapid visualization and measurement data for further digital processing.

2 Materials and methods

The middle infrared (MIR) scanning setup used here is based on a flying-spot scanner [10]. The measurement setup basically consists of two lasers, a focusing unit, an agile mirror system and a detector (Figure 3.1). The laser beams are deflected one-dimensionally by the agile mirror unit. The sample is displaced orthogonally to the deflected laser beam by means of a translation stage. This method and confocal signal acquisition reduce image distortion. The maximum measuring area is 50 cm^2 with a spatial resolution of $20 \text{ }\mu\text{m}$. The sample is scanned at a sampling rate of 300 kS/s . At this scanning speed, the maximum measuring area is scanned within 50s. This is the measurement time for each individual laser.

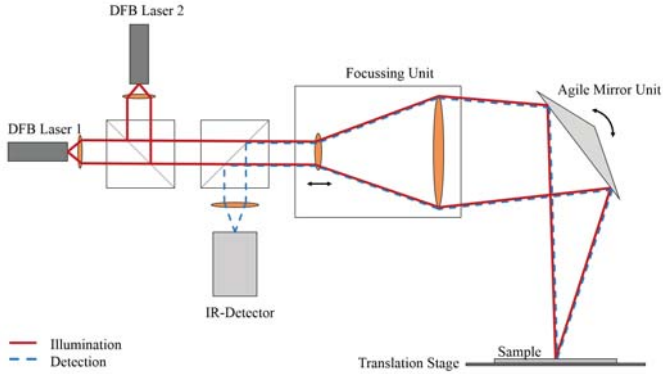


Figure 3.1: Schematic representation of the MIR scanner. The laser beam is focused on the sample by the agile lens unit (Focussing Unit). The laser light is deflected by the agile mirror unit orthogonally to the deflection direction of the laser beam, the translation stage operates. The detector is confocally mounted at the optical path of the laser light.

The acquired measurement data are sorted by complex algorithms and assembled as a measurement image. The resulting and calculated measurement images represent the absorption properties at the measuring target. The following sequence of measurements demonstrates the absorption properties of human body fat. On these, 3-dimensional finger fat marks are created. Each individual has a different concentra-

tion of body fat [11], so a standard reference is used. Wool wax (adepts lanae anhydricus; antioxidant = max. 200 ppm BHT), in its properties approximately similar to human body fat, is used for reference.

3 Theory/Calculation

The Lambert-Beer law in MIR spectroscopy is applied to the MIR scanner presented here. The measured absorption A is composed of the negative decadic logarithm of the transmission T (Equation 3.1). In this case, the absorption is proportional to specific sample concentration c , thickness of sample material d and material-dependent extinction coefficient ϵ [12].

$$A = -\log_{10}(T^2) = -\log_{10}\left(\frac{I_{Laser1}}{I_{Laser2}}\right)^2 = \epsilon c d_{Substance} \quad (3.1)$$

The transmission T is determined by the ratio of the two lasers. Here, the exponential dependence of the transmission represents the twofold sample passage of the laser light. This is comparable to DRIFTS (diffuse reflectance infrared fourier transform spectroscopy). The absorption A can be calculated by transforming the transmission. Based on this assumption, conclusions can be drawn as to the measured material thickness $d_{Substance}$ at a constant concentration c of a substance.

In theory, the aim is to set one of the two lasers (Laser 1) to the wavelength of a transmission minimum and to set the second laser (Laser 2) to a transmission maximum. Since the extremes are accompanied by rapid increases or decreases of the flanks, it is not always possible to adjust the laser exactly to theoretical values. Therefore, it is of decisive importance to locate a laser (Laser 1) within a band exhibiting an increased absorption coefficient. In contrast, the second laser (Laser 2) has to be located in a range that has a lower absorption level than Laser 1. In Figure 3.2, the lasers used in this work are highlighted in the spectral transmission range of fat and oil. Laser 1 is set to the wavelength $\lambda = 3417$ nm (2926 cm $^{-1}$) and laser 2 to the wavelength $\lambda = 3584$ nm (2797 cm $^{-1}$). The samples presented in Figure 3.2 show the C-H vibration the lasers are adjusted to. The adjusted wavelengths therefore absorb substances from triglycerides in combination with long-chain fatty acids.

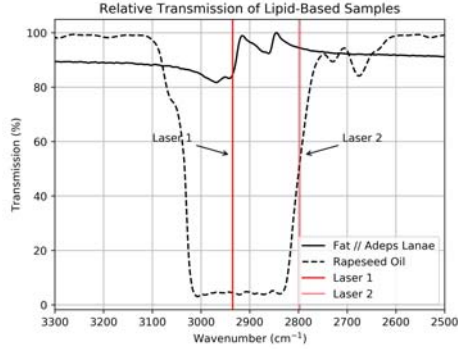


Figure 3.2: Relative transmission of fat (*Adeps Lanae*) and rapeseed oil. Both exhibit differences in transmission at wavenumbers from 2500 cm^{-1} to 3300 cm^{-1} . The wavenumbers of the lasers are located in the band between 2980 cm^{-1} and 2700 cm^{-1} . Laser 1 assumes the wavenumber 2926 cm^{-1} and Laser 2 the wavenumber 2797 cm^{-1} .

4 Results and Discussion

The scan results presented in Figure 3.3 depict the measurement results with the MIR scanner in raw data format. Figure 3.3a) represents the scan result for Laser 1 with wavelength 3417 nm . In contrast, Figure 3.3b) shows the scan result of Laser 2 with wavelength 3584 nm . Figure 3.3c) shows the calculated transmission T^2 as an enlarged section of the measurement results. Based on this calculated and magnified section, the profile thickness is evaluated and demonstrated in the following.

These measurement data are linked to a calibration subsequently (Figure 3.4). Hence, the absorption of different layer thicknesses is determined for both wavelengths. After scanning the layer thicknesses, a linear calibration curve of wool wax fat is generated. The related relative transmission of both laser wavelengths as a function of the penetration depth is shown in Figure 3.4a).

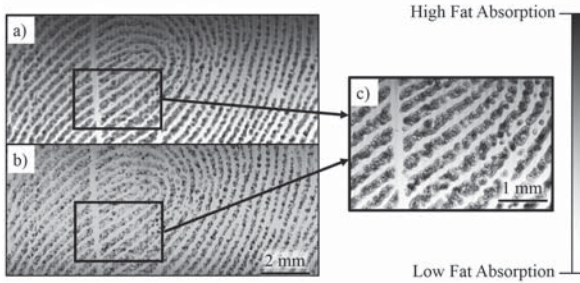


Figure 3.3: Scan result of a human fingerprint. a) Scan of the fingerprint with wavelength 3417 nm. b) Scan of the fingerprint with wavelength 3584 nm. c) Section of calculated transmission T^2 (zoomed).

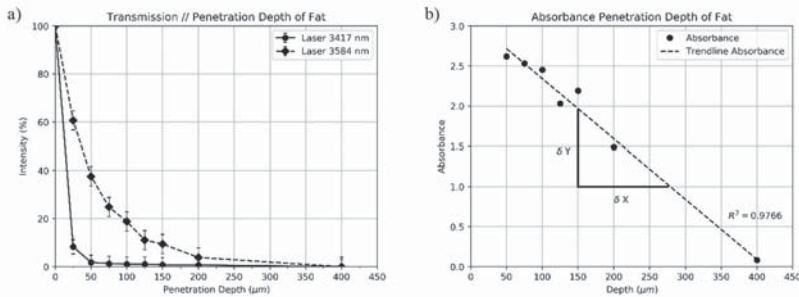


Figure 3.4: Depiction of the penetration depth for fat. a) The intensity of the two wavelengths decreases with increasing penetration depth. b) Determination of the penetration depth using a calibration model for fatty substances (especially finger fat).

By determining the penetration depth, a calibration is performed enabling the penetration depth to be assigned to an absorption value. The absorption is obtained by applying Equation 3.1 to the determined penetration depth values as shown in Figure 3.4a). As a result, a linear calibration curve can be generated for layer thicknesses between 25 μm and 400 μm (Equation 3.2). The calibration curve is illustrated in Figure 3.4b). For a penetration depth less than 25 μm, the coefficient of determination decreases, this is equivalent to a nonlinearity in

a calibration curve associated with it. This is due to insufficient absorption at this layer thickness. In contrast, the maximum penetration depth to be determined is limited to 200 μm . The signal-to-noise ratio (SNR) is not sufficient for data processing at higher penetration depths. Theoretically, a penetration depth of up to 400 μm could be achieved. By linking the calibration curve with Lambert-Beer, an unknown layer thickness d can be calculated from the measured absorption A (Equation 3.3).

$$A = md + b \quad (3.2)$$

$$d = \left(\frac{A - b}{m} \right) \quad \rightarrow \text{with : } m = \frac{\delta d}{\delta A} = \frac{d_n - d_{n-1}}{A_n - A_{n-1}} \quad (3.3)$$

This mathematical method is applied to the following scan results of Figure 3.3c). A layer thickness is assigned to each image pixel and related to the absorption information. This results in a topographic image of the fingerprint. Image processing procedures are used to assign a visual colour to each layer thickness. The calculated scan result is presented in Figure 3.5.

Figure 3.5 demonstrates an average profile height between 150 μm and 200 μm for this fingerprint. In addition, it is shown that the background of the fingerprint is eliminated by calculating the absorption differences (Equation 3.1). For improved visualization, Figure 3.6 shows the height profile on the plot line (PL) marked in Figure 3.5. The widths, the heights and distances between the papillary ridges can be determined directly from such a plot.

Figure 3.6 indicates that the papillary ridge and the associated heights of the finger fat are not contiguous. In addition, peaks are recognizable by increasing and decreasing profile heights. This is due to direct reflections from structural changes. To reduce the associated increase in intensity and the resulting falsified profile height, a smoothing filter (Savitzky-Golay filter) can be superimposed on the structure [13]. This generates a more homogeneous continuous height of the fingerprint. The disadvantage is the elimination of interrupted structures within the papillary ridge and the associated loss of information.

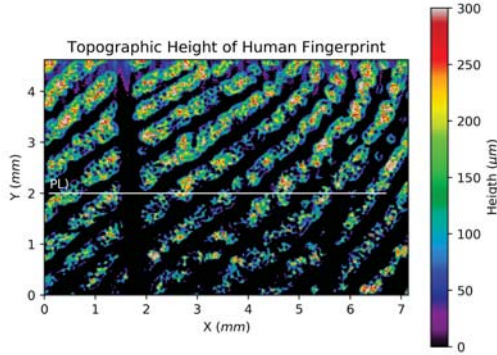


Figure 3.5: Absorption image of the fingerprint depending on the depth information of the fat layer. The plot line (PL) indicates a single line represented in Figure 3.6.

5 Conclusions

In this work we proved the possibility to visualize fingerprints with the MIR scanner and assign topographic information to the generated image. A scan rate of 300 kS/s in combination with the spatial scan resolution of 20 μm provides fast, high spatial resolution scan results. Here we rely on the absorption measurement with two different wavelengths, exhibiting absorption differences of long-chain C-H bonds. In addition, we demonstrated a calibration method based on known mathematical correlations that enables conclusions about the thickness of finger mark. The results are generated immediately from the measured data. Thus, the fingerprint is displayed as an image with height information of the analyzed sample. The resulting image, containing the 3-dimensional structures of the fingerprint, can thus be passed on to the forensic analysis [3] for further processing. Further test series for thin layers ($< 25 \mu\text{m}$) will be performed with nonlinear regressions. In addition, an adjustment of smoothing algorithms is necessary, depending on the examined structure and associated interruptions. Fingerprints on various surfaces have to be checked as well.

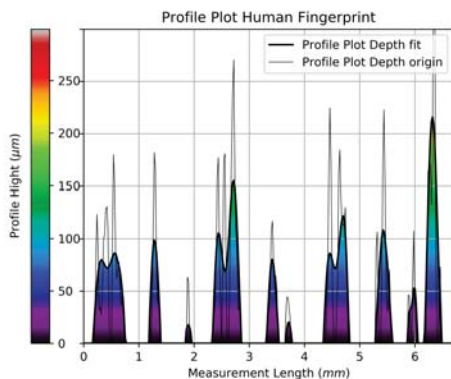


Figure 3.6: Representation of the profile depth of the scanned fingerprint as an original and smoothed detection signal with colour assignment of the profile height.

Furthermore, this measuring principle is applicable to oil and associated oil residues. For this purpose, a new calibration has to be performed for the respective oil, as this absorbs differently in liquid form as shown in Figure 3.2.

Acknowledgement

The German Federal Ministry of Economics and Energy (BMWi), supported by the Association of Industrial Research Associations (AiF Project GmbH, Grant No: ZF4168604TS8, ZF4560205TS8), have sponsored this project. The authors would also like to thank the Karl-Völker-Stiftung (KVS) for its financial support.

References

1. S. C. Dass, "Fingerprint-based recognition," *International Statistical Review*, vol. 81, no. 2, pp. 175–187, 2013.
2. A. de Jongh, A. R. Lubach, S. L. Lie Kwie, and I. Alberink, "Measuring the rarity of fingerprints patterns in the dutch population using an extended classification set," *Journal of forensic sciences*, 2018.
3. N. Yager and A. Amin, "Fingerprint verification based on minutiae features: a review," *Pattern Analysis and Applications*, vol. 7, no. 1, pp. 94–113, 2004.
4. P. H. R. Ng, S. Walker, M. Tahtouh, and B. Reedy, "Detection of illicit substances in fingerprints by infrared spectral imaging," *Analytical and bioanalytical chemistry*, vol. 394, no. 8, pp. 2039–2048, 2009.
5. C. G. Worley, S. S. Wiltshire, T. C. Miller, G. J. Havrilla, and V. Majidi, "Detection of visible and latent fingerprints using micro-x-ray fluorescence elemental imaging," *Journal of forensic sciences*, vol. 51, no. 1, pp. 57–63, 2006.
6. M. Najdoski, S. Oklevski, and G. Stojković, "A simple chemical method for visualization of sebaceous fingerprints on unfired cartridge cases by prussian blue deposition," *Russian Journal of Applied Chemistry*, vol. 88, no. 11, pp. 1896–1901, 2015.
7. Y. Wang, J. Wang, Q. Ma, Z. Li, and Q. Yuan, "Recent progress in background-free latent fingerprint imaging," *Nano Research*, pp. 1–20, 2018.
8. R. Bhargava, R. S. Perlman, D. C. Fernandez, I. W. Levin, and E. G. Bartick, "Non-invasive detection of superimposed latent fingerprints and interridge trace evidence by infrared spectroscopic imaging," *Analytical and bioanalytical chemistry*, vol. 394, no. 8, pp. 2069–2075, 2009.
9. J.-H. Rabe, D. A. Sammour, S. Schulz, B. Munteanu, M. Ott, K. Ochs, P. Hohenberger, A. Marx, M. Platten, C. A. Opitz *et al.*, "Fourier transform infrared microscopy enables guidance of automated mass spectrometry imaging to predefined tissue morphologies," *Scientific reports*, vol. 8, no. 1, p. 313, 2018.
10. N. Ramanujam, J. Chen, K. Gossage, R. Richards-Kortum, and B. Chance, "Fast and noninvasive fluorescence imaging of biological tissues in vivo using a flying-spot scanner," *IEEE Transactions on biomedical engineering*, vol. 48, no. 9, pp. 1034–1041, 2001.
11. R. Ostlund Jr, J. Yang, S. Klein, and R. Gingerich, "Relation between plasma leptin concentration and body fat, gender, diet, age, and metabolic covari-

- ates," *The Journal of Clinical Endocrinology & Metabolism*, vol. 81, no. 11, pp. 3909–3913, 1996.
12. D. Swinehart, "The beer-lambert law," *Journal of chemical education*, vol. 39, no. 7, p. 333, 1962.
 13. P. A. Gorry, "General least-squares smoothing and differentiation by the convolution (savitzky-golay) method," *Analytical Chemistry*, vol. 62, no. 6, pp. 570–573, 1990.